https://erjm.journals.ekb.eg
ISSN: 1110-1180

DOI: ---------

ERJ
Engineering Research Journal
Faculty of Engineering
Menoufia University

Performance Analysis of a Photovoltaic Source Connected to the Utility Grid

Adel A. Abou El-Ela [1], Sohir M. Allam [1], Asmaa F. Shehab [2*]

[1] *Department of Electrical Engineering, Faculty of Engineering, Menoufiya University, Egypt.*
[2] *New and Renewable Energy Authority (NREA), MOERE, Cairo, Egypt,*
[*] *(Corresponding author: asmaafouad47@yahoo.com)*

ABSTRACT
Photovoltaic (PV) technology is in the forefront of renewable energy and gained a lot of attention as a very promising green technology towards direct solar energy conversion to electricity. So, enhancing the PV solar cell performance is an important target for improving PV system performance. In this paper, a recent algorithm called Arithmetic Optimization Algorithm (AOA) is proposed to find the optimal PV model parameters to build a Simulink model for an actual case study of the New and Renewable Energy Authority (NREA) 42 kW PV system. The results of the proposed AOA are compared with that obtained by means of particle swarm optimizer (PSO). Also, performance analysis is introduced for the practical measurements from the grid-connected PV system. Energy is measured for the installed PV system at the NREA in Cairo and the proposed system is simulated during daily weather conditions to test its operational performance based on simulation results. The system is installed to produce 2.17 MWh/year of energy production. Based on the optimal parameters for the study module using the proposed AOA, the detailed Simulink model of small-scale 42 kW PV system is accurately designed and connected to the utility grid. Furthermore, the output energy of the investigated system, with the aid of the proposed AOA, is efficiently estimated compared with the actual energy generated of case study.

Keywords: *photovoltaic system, Arithmetic Optimization Algorithm, Particle Swarm Optimization, Simulink model, performance analysis of PV, practical parameters measurement.*

1. Introduction

Renewable energy technologies account for a larger percentage of the power generating mix in order to reduce reliance on oil and play an important role in reducing Greenhouse Gas Emissions (GHG) degrees of concentration stability mitigation of climate change [1].

One of the most widespread sources in the world, especially in Egypt, is solar energy, as Egypt is one of the solar belt countries which is characterized by arid climatic conditions [2,3]. As of 2019, the solar energy capacity in Egypt amounted to 1,668 megawatts. This represented a sharp increase of roughly 116.3 % from the preceding year [4,5], which led to increase the research in the field of PV stations [6].

In this context a considerable number of algorithms have been applied to get the optimal parameters of PV models, like elephant herd algorithm [7], marine predator [8], supply-demand optimization algorithm [9], ecosystem optimization algorithm [10], elephant herd optimization plus closed loop particle swarm optimization algorithm [11], multiple learning backtracking search algorithm [12].

These literatures have shown amazing effort for estimating optimal PV models parameters. None of the applied algorithms obtained a comprehensive solution as the process of random distribution differs from one algorithm to another.

In this paper, the best three PV model parameters are extracted using a suggested optimization approach called Arithmetic Optimization Algorithm (AOA) [13]. A PV model's mathematical model is indicated, and a series of equations is used to illustrate the (I-V) characteristic equation of a PV model.

In addition, a MATLAB code is employed to simulate the parameters of PV cells based on analytical expressions and determine the values of these parameters using AOA. Also, experimental data is used to plot the (P-V) and (I-V) characteristic curves. Then a comparison between these curves and that deduced from PSO algorithm, as another optimization algorithm, is introduced. Besides a Simulink model of NREA 42 KW PV power system is constructed to explain the system performance versus the actual one.

The main contributions of this study are as follows:

- A recent algorithm of AOA is proposed and effectively employed to find the optimal PV model parameters.
- Higher performance of the proposed AOA is demonstrated compared with the well-known PSO.
- Based on the optimal parameters for the study module using the proposed AOA, the detailed Simulink model of small-scale 42 kW PV system is accurately designed and connected to the utility grid.
- A performance analysis is carried out for the practical measurements from the grid-connected PV system.
- Furthermore, the output energy of the investigated system, with the aid of the proposed AOA, is efficiently estimated compared with the actual energy generated of case study.

The rest of the paper is organized as follows: Section 2 illustrates the problem formulation including the equivalent circuits of different PV models. Section 3 describes the structure of grid connected PV of NREA 42 kW PV Power System. Section 4 shows the employed optimization techniques. Section 5 investigates the results and discussions while the conclusions are drawn in the last section.

2. Problem Formulation

2.1. Equivalent circuit of PV model

Photovoltaic can be represented as commonly by means of five parameters Single Diode Model (SDM), seven parameters Double Diode Model (DDM) and nine parameters Triple Diode Model (TDM) which will be investigated. The operations of these models are based on variation of the surrounding conditions of irradiance, temperature and the number of model parameters as will be discussed in the following subsections

.

2.2. Five parameters of single diode model (SDM)

The mathematical formulation of the five parameters SDM is clarified through a set of analytical equations. However, the output current equation is a function of five unknown parameters $(I_{ph}, I_{o1}, n_1, R_s, R_{sh})$ in which I_{ph} is defined photo generated current and it is dependent on the ambient temperature and the irradiance, I_{o1} is the first diode reverse saturation current with diode ideality factor n_1 which has a range between 1 to 2. R_s is the series resistance of a solar cell represents the losses due to connections and R_{sh} is shunted across the diode due to the p-n junction leakage current. Fig.1 illustrates the five parameters of SDM [14,15].

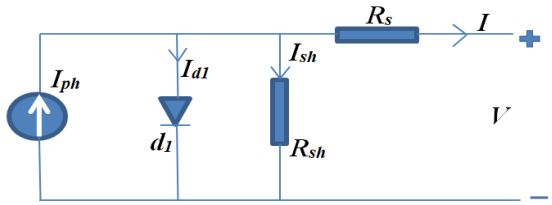

Figure 1- Equivalent circuit of the single-diode photovoltaic model (SDM)

Applying Kirchhoff's current law to the equivalent circuit shown in Figure (1), the output current that indicates the (I-V) characteristic equation is as follow [16]:

$$I = I_{ph} - I_{d1} - I_{sh} \quad (1)$$

Where I represents the SDM output current in ampere (A), I_{ph} is photo generated current and the shockley diode current across the first diode (I_{d1}) can be expressed as follow [17,18]:

$$I_{d1} = I_{o1}[exp^{\frac{q(V+IR_s)}{n_1 K T_c}} - 1] \quad (2)$$

Where I_{o1} represents first diode reverse saturation current in A, q and k are charge of an electron equal to $1.602 * 10^{(-19)}$ and Boltzmann constant ($1.38 * 10^{(-23)}$J/°k) respectively, V is the voltage generated in the PV SDM in Volt (V), R_s is series resistance in Ohm (Ω), n_1 is the ideality factor of the first diode and T_c is the operating temperature of PV SDM in Kelvin (k).

Applying Kirchhoff's voltage law, the current (I_{sh}) across the shunt resistor (R_{sh}) can be calculated as follow [19,20]:

$$I_{sh} = [\frac{V+IR_s}{R_{sh}}] \quad (3)$$

Substituting (2) and (3) in (1), the output current of the PV SDM cell is obtained as [21,22]:

$$I = I_{ph} - I_{o1}[exp^{\frac{q(V+IR_s)}{n_1 K T_c}} - 1] - [\frac{V+IR_s}{R_{sh}}] \quad (4)$$

The variation of both ambient temperature and radiation effect the values of the photo generated, as [23]:

$$I_{ph} = I_{phr} + \mu(T_c - T_{cr})G/G_r \quad (5)$$

Where I_{phr} indicates photo generated current at standard test conditions which equals (I_{sc}) in A, μ is the temperature coefficient of short-circuit current in (A/K), T_{cr} is the reference temperature of PV SDM which equals 298°K, G and G_r represent radiation on PV SDM at given conditions and radiation at standard conditions in W/m^2.

The saturation current relies on the PV ambient temperature, as [24,25]:

$$I_{o1} = I_{o1_{ref}} \left(\frac{T_c}{T_{cr}}\right)^3 e^{\left[\frac{qE_g}{n_1 k}\left(\frac{1}{T_{cr}} - \frac{1}{T_c}\right)\right]} \quad (6)$$

Where, ($I_{o1_{ref}}$) corresponds to the first diode reverse saturation current at standard test conditions, which

is calculated as follow [25]:

$$I_{o1_{ref}} = \frac{I_{sc}}{\left(e^{\frac{q(V_{OC})}{N_S n_1 KT_C}} - 1\right)} \quad (7)$$

Where E_g is the band-gap energy (1.12eV for Si, 1.35eV for GaAs) and V_{oc} is the open circuit voltage in (V). Also the value of R_s can be calculated as:

$$R_s = \frac{N_s n_1 V_T \ln\left(1 - \frac{I_{mpp}}{I_{sc}}\right) + V_{oc} - V_{mpp}}{I_{mpp}} \quad (8)$$

where, V_T is the thermal voltage, because of its exclusive on dependent on temperature and can be obtained through the following approximation [26]:

$$V_T = \frac{KT_c}{q} \quad (9)$$

Also V_{mpp}, I_{mpp} indicate voltage at maximum power point (V) and current at maximum power point (A).

The ideality factor (n_1) can be analytically calculated from equation (9) as:

$$n_1 = \frac{V_{mpp} - V_{oc} + R_s * I_{mpp}}{V_T \ln\left[\left(I_{sc} - I_{mpp} - \frac{V_{mpp} + R_s * I_{mpp}}{R_{sh}}\right)/\left(I_{sc} - \frac{V_{oc}}{R_{sh}}\right)\right]} \quad (10)$$

Commonly, increasing the output power is developed by connecting number of PV cells in series, which are defined as N_s, and some in parallel known as N_p. So, the current–voltage characteristic equation of a PV SDM module is shown as follow [27]:

$$I_m = N_s I_{ph} - N_p I_{o1}\left[e^{\frac{q\left(\frac{V_m}{N_s} + \frac{I_m R_s}{N_p}\right)}{n_1 KT_C}} - 1\right] - \left[\frac{V_m\left(\frac{N_p}{N_s}\right) + I_m R_s}{R_{sh}}\right] \quad (11)$$

Where I_m, V_m represent the output current of the PV module in (A) and the output voltage of the PV module in (V) [28].

2.3. Seven parameters for double diodes model (DDM)

Figure (2) shows the equivalent circuit of seven parameters of DDM where an additional diode is added in parallel with the current source with another ideality factor [29,30]:

$$I = I_{ph} - I_{d1} - I_{d2} - I_{sh} \quad (12)$$

Where, I_{d2} is the current across the additional parallel diode as:

$$I_{d2} = I_{o2}\left[exp^{\frac{q(V+IR_S)}{n_2 KT_C}} - 1\right] \quad (13)$$

Where, I_{o2} is the reverse saturation current of additional second diode, n_2 is the second diode ideality factor. The seven unknown parameters are $[I_{ph}, I_{o1}, I_{o2}, n_1, n_2, R_s, R_{sh}]$.

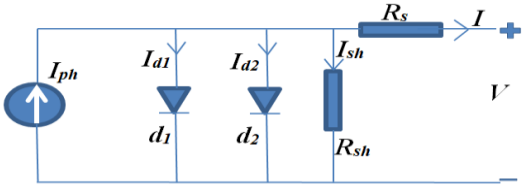

Figure 2- Equivalent circuit of PV DDM

2.4. Nine parameters for triple diodes model (TDM)

The equivalent circuit of TDM is described in Figure (3), in which three diodes are connected in parallel with the current source each one has the reverse saturation current and ideality factor, so the equation with nine parameters $[I_{ph}, I_{o1}, I_{o2}, I_{o3}, n_1, n_2, n_3, R_s, R_{sh}]$ that describes the output current can be deduced as follow [30,31]:

$$I = I_{ph} - I_{d1} - I_{d2} - I_{d3} - I_{sh} \quad (14)$$

Where, I_{d3} is the current pass through third diode which is calculated as:

$$I_{d3} = I_{o3}\left[exp^{\frac{q(V+IR_S)}{n_3 KT_C}} - 1\right] \quad (15)$$

Where, I_{o3} is the reverse saturation current and n_3 is the ideality factor of the third diode. Taking into consideration the nine parameters of TDM, it is better to improve the accuracy of the model.

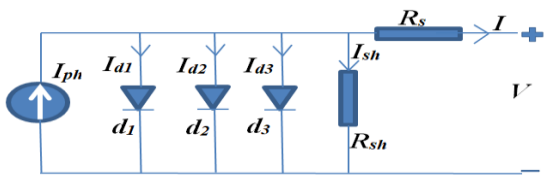

Figure 3- Equivalent circuit of PV TDM

2.5. Optimal Extraction of PV Parameters

The parameters of PV model are $[I_{ph}, I_{o1}, I_{o2}, I_{o3}, n_1, n_2, n_3, R_s, R_{sh}]$, so the main objective of this modeling is to enable the solar PV model to predict the output characteristics of the PV module. In order to reduce the difference between predicted and actual output characteristics of the PV module, one has to find the optimized parameters of the solar PV model. This can be done by using various optimization techniques.

The root mean square error (RMSE) is chosen as the objective or fitness function that can be calculated as:

$$RMSE = \sqrt{\frac{1}{N}\sum_{i=1}^{N}(I_i - I_{i,exp})^2} \quad (16)$$

Where, $I_{i,exp}$ refers to the experimental readings of the output current, N counts the number of these values, and I_i is the estimated current of SDM, DDM, and TDM.

Each model current is a function of unknown variables (P), so the objective functions of the three models can be expressed as a function of the following unknown parameters:

For SDM, P = $I_{ph}, I_{o1}, n_1, R_s, R_{sh}$

For DDM, P= $I_{ph}, I_{o1}, n_1, R_s, R_{sh}, I_{o2}, n_2$

For TDM, P = $I_{ph}, I_{o1}, n_1, R_s, R_{sh}, I_{o2}, n_2, I_{o3}, n_3$

3. Structure of Grid Connected PV of NREA 42 kW PV Power System

3.1. Experimental Test

The Mono Crystalline 390 – 430 TS6S96 (TS-S410) PV module is tested in NREA laboratory which is the only one in the Middle East that performs many laboratory tests of PV models and issues certificates of the results.

The test is performed in according with International Standard IEC 61215. The objective of this test sequence is to determine the electrical and thermal characteristics of the module and to show, as far as is possible within reasonable constraints of cost and time, that the module is capable of withstanding prolonged exposure in climates.

a) As a first step of the laboratory test, the PV module should be connected correctly in a dark test chamber as shown in Figure (4), where in the back front of the module the temperature sensor is connected and called (Transducer) as shown in Figure (5). Through this Transducer the current, voltage and temperature are converted into digital signals, also both a tracer for measuring and analyzing the (I-V) characteristics of photovoltaic specimens (solar cells, solar modules) and the module are connected to the monitor cell on the right side to measure the irradiance level during the (I-V) curve measurement.

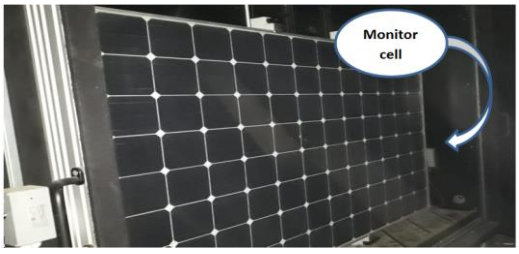

Figure 4- Mono Crystalline 390 – 430 TS6S96 (TS-S410) test module

Figure 5- Voltage, current and temperature transducers

b) Electronic xenon flasher used to generate sun light within a short duration (flash) as in Figure (6). The flash box is equipped with a light-intensity feedback sensor to enable adaptive light-intensity control.

c) When the module is exposed to radiation similar to sunlight, the module is represented by a current source, and connected with an electronic load as in Figure (7). So, an electric current passes directly proportional to the solar radiation and through a computer software program.

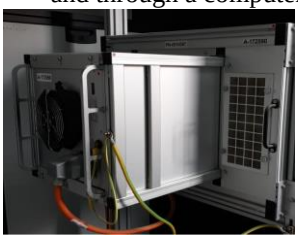

Figure 6- Electronic xenon flasher

Figure 7- Electronic load connected to the module

d) The temperature from the thermo unit can be adjusted and after that the test is started. However, the test results are appeared on the computer screen.

3.2. Model Structure of Grid Connected PV of NREA 42 kW PV Power System

The layout of photovoltaic source connected to the utility grid is described in Figure (8), in which a number of complementing components exist. The first part is the series and parallel PV modules that convert the radiation into DC output power, the second part in the three-phase inverter compacted with LC filter to obtain smooth output waveform. Also the three-phase transformer is responsible for converting the DC power to AC power to be injected into the utility grid [32-34].

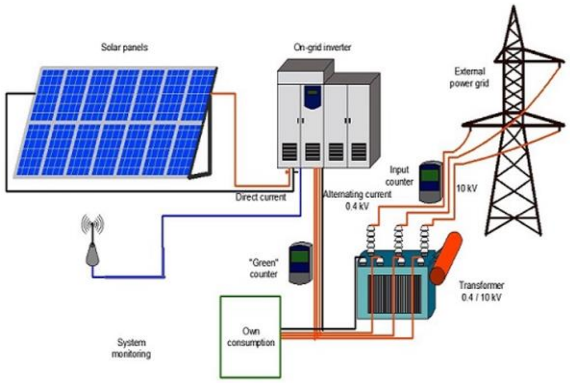

Figure 8- Grid-connected PV system

3.3. Simulink Model of Grid Connected PV of NREA 42 kW PV Power System

This paper presents a Simulink model for NREA 42 kW PV power system connected to the utility grid as shown in Figure (9). This model is composed of 104

module of type Mono Crystalline 390 – 430 TS6S96 (TS-S410) PV module with optimal parameters extracted from the AOA.

As the RMSE between the three models of the proposed module are very convergent. So SDM is used due to simplicity and less computational time to design a Simulink model with optimal parameters equal $[I_{ph}, I_{o1}, n_1, R_s, R_{sh}]$ of 8.95376, 0.0348066, 0.0003777, 1.26126 and 33.7929, respectively as shown in Figure (10).

The part of series/parallel modules of the system is defined as the DC part with a Simulink model as illustrated in Figure (11). The inverter configuration and its filter are illustrated as in Figure (12)and Figure (13).

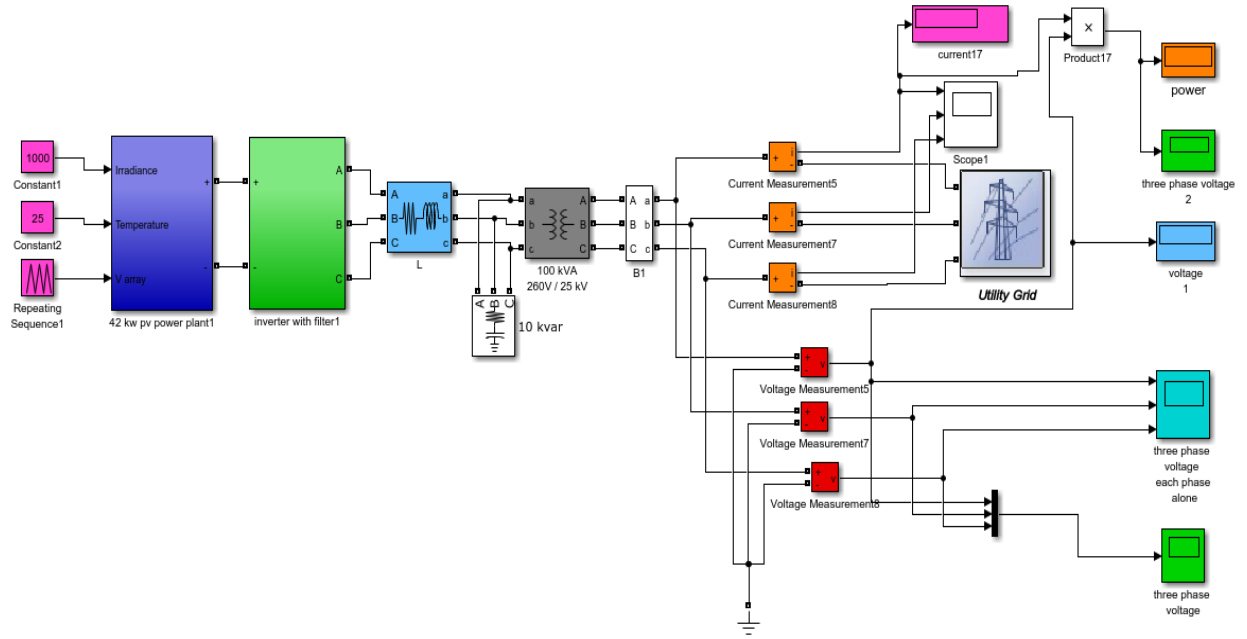

Figure 9- Simulink model of NREA 42 kW PV system

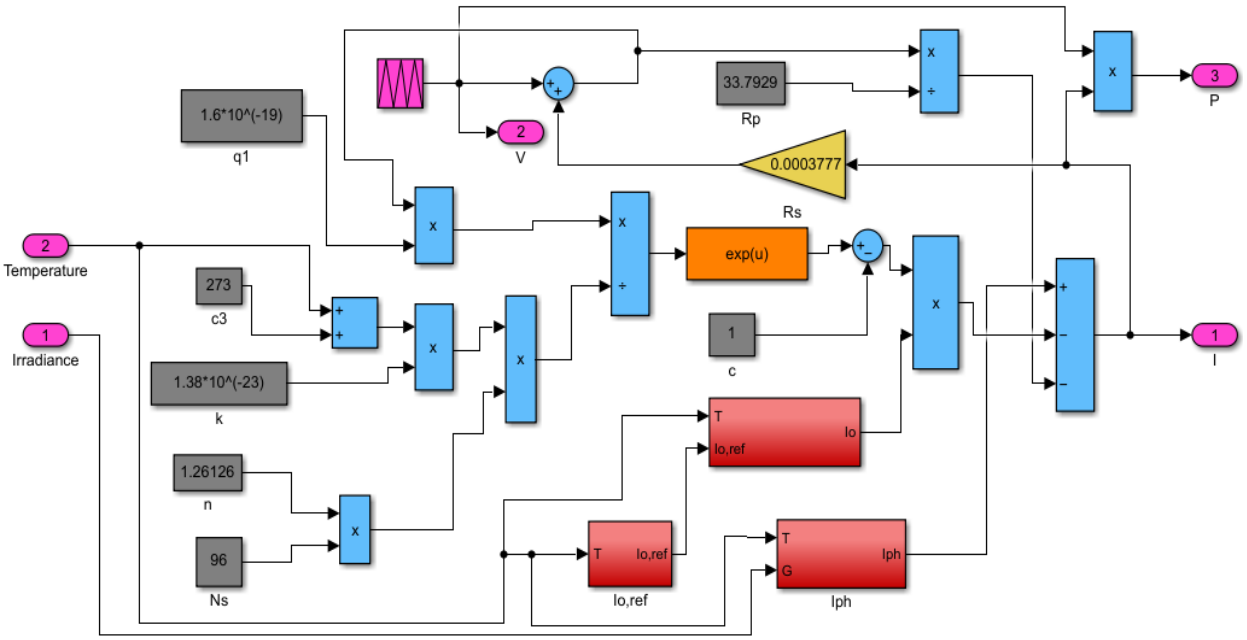

Figure 10- Simulink model of Mono Crystalline 390 – 430 TS6S96 (TS-S410) PV module

3.4. DC part of 42 kW PV power system

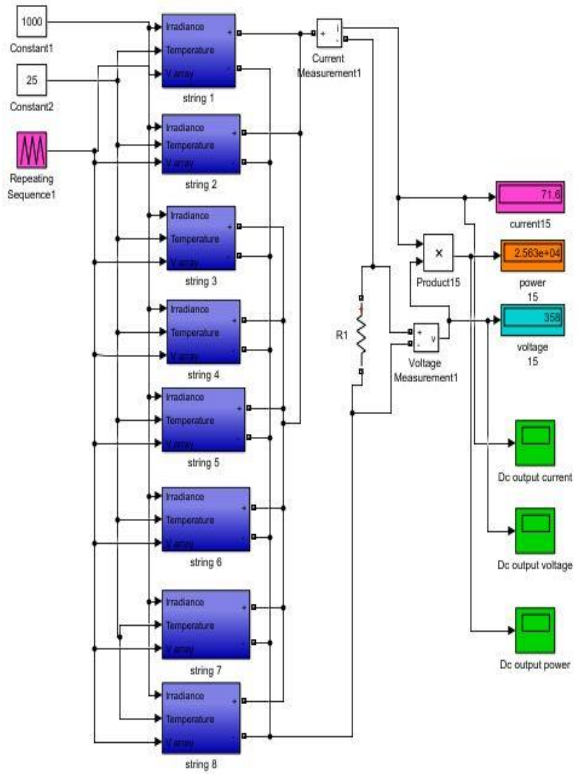

Figure 11- Simulink model of Parallel strings

3.5. Simulink model of Three-phase inverter

Converting the DC output power wave form to AC is an essential stage which is performed through three-phase inverter as in Figure (12). The inverter type is KACO, Powador with maximum efficiency equals 97.8 % with a data sheet shown in Appendix (A) [33].

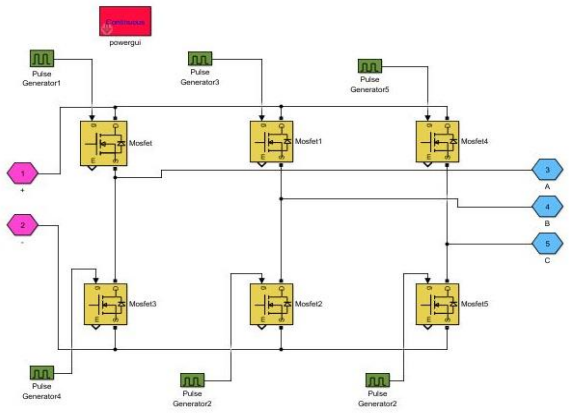

Figure 12- Simulink model of Inverter configuration

3.6. Configuration of LC filter

Usually the output waveform produced from inverter has much ripples, so the presence of a filter with series connected inductance and shunt capacitors is necessary to get a smooth three-phase output waveform as illustrated in Figure (13) [34].

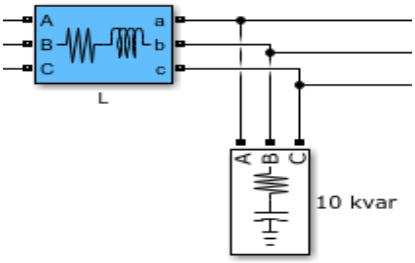

Figure 13- Simulink model of the filter circuit

4. Employed Optimization Techniques

In this section, two optimization techniques are used as proposed Arithmetic Optimization Algorithm (AOA) and particle swarm optimization algorithm to find the optimized parameters of Mono Crystalline 390 – 430 TS6S96 (TS-S410) PV module.

4.1. Proposed AOA

The Arithmetic Optimization Algorithm (AOA) is proposed as a recent algorithm that can achieve the objective function through two stages called exploration and exploitation. In the AOA code, the calculations start with the initial matrix of random solutions (X), every iteration begins with the optimal solution from the previous iteration. AOA has some equations through which the optimization process is performed as follow:

$$MOA(C\_Iter) = Min + C\_Iter * (\frac{Max-Min}{M\_Iter}) \quad (17)$$

Where, MOA(C_Iter) indicates the value of the objective function value at the t[th] iteration, C_Iter is the present iteration. Min and Max denote the minimum and maximum values of the accelerated function, respectively.

4.1.1. Exploration phase

In this phase, a set of equations discover the near-optimal solution after many iterations.

$$x_{i,j}(C_{Iter}+1) = \begin{cases} best(x_j) \div (Mop+\varepsilon) \times ((Ul_j - Ll_j) \times \mu + Ll_j), r_2 < 0.5 \\ best(x_j) \times Mop \times \left((Ul_j - Ll_j) \times \mu + Ll_j\right), \quad otherwise \end{cases} \quad (18)$$

Where, $x_i(C\_Iter+1)$ is the i[th] solution in the next iteration, $x_{i,j}(C\_Iter+1)$ is the j[th] position of the i[th] solution at the present iteration, and $best(x_j)$ denotes the j[th] position in the best-obtained solution so far. ε is an integer number with a small value, Ul_j and Ll_j denote the values of the upper limit and the value of the lower limit of the j[th] position, respectively. μ is a constant coefficient equals to 0.5 to adopt the calculations.

$$MOP(C\_Iter) = 1 - \frac{C\_Iter^{1/\alpha}}{M\_Iter^{1/\alpha}} \quad (19)$$

Where, Math Optimizer probability (MOP) is a coefficient, MOP(C_Iter) means the function value at the t[th] iteration, and C_Iter means the current iteration

and (M_Iter) indicates number of iterations, that the maximum number of α is equal to 5.

4.1.2. Exploitation phase

The exploitation stage equation is as follow:

$$x_{i,j}(C_{Iter}+1) = \begin{cases} best(x_j) - Mop \times \left((Ul_j - Ll_j) \times \mu + Ll_j\right), & r_3 < 0.5 \\ best(x_j) + Mop \times \left((Ul_j - Ll_j) \times \mu + Ll_j\right), otherwise \end{cases} \quad (20)$$

Eventually, the AOA algorithm is stopped by reaching the satisfaction of the end criterion. The intuitive and detailed process of AOA is shown in Figure (14).

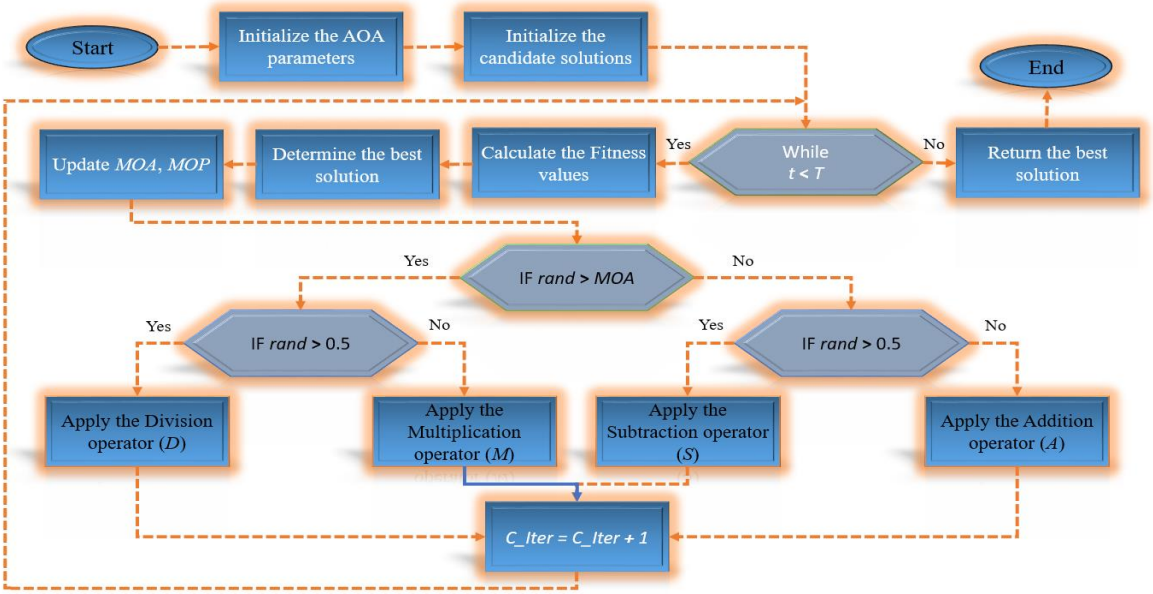

Figure 14- Flow chart of the proposed Arithmetic Optimization Algorithm (AOA).

4.2. PSO

PSO is a population-based swarm intelligence algorithm. PSO algorithm uses the physical movements of the individuals in the swarm that has a flexible and well-balanced mechanism to enhance and adapts to the global and local exploration abilities [35].

The PSO algorithm first randomly initializes a swarm of particles. The position of each individual (called particle) is represented by a d-dimensional vector in problem space $s_i = s_i(1), s_i(2), \ldots\ldots, s_i(d)$, i = 1,2, ..., N_{pop}, where N_{pop} is the population size, and its performance is evaluated on the predefined fitness function. Thus, each particle is randomly placed in the d-dimensional space as a candidate solution. The velocity of the i^{th} particle $v_i = v_i(1), v_i(2), \ldots\ldots, v_i(d)$ is defined as the change of its position. The flying direction of each particle is the dynamical interaction of individual and social flying experience.

The algorithm completes the optimization through following the personal best solution of each particle and the global best value of the whole swarm.

Each particle adjusts its trajectory toward its own previous best position and the previous best position attained by any particle of the swarm, namely p_i and p_g. In each iteration, the swarm is updated by the following equations [35].

$$v_i(t+1) = v_i(t) + c_1 rand_1\left(p_i - s_i(t)\right) + c_2 rand_2 \quad (21)$$

$$s_i(t+1) = s_i(t) + v_i(t+1) \quad (22)$$

5. Results and Discussions

5.1. Simulation Results of AOA application for PV models

This section explained application of the proposed Arithmetic Optimization Algorithm (AOA) on the Mono Crystalline 390 – 430 TS6S96 (TS-S410) PV SDM, DDM and TDM models to extract the optimal parameters, the constraints limits as a range of values between minimum and maximum limits are summarized in Table (1).

Table 1- Parameters limits for Mono Crystalline 390 – 430 TS6S96 (TS-S410) PV module

Parameters	Lower limit	Upper limit
I_{ph}	0	9
$I_{s1}, I_{s2}, I_{s3}(\mu A)$	0	1
R_s	0	0.5
R_{sh}	0	100
n_1, n_2, n_3	1	2

The results of the proposed AOA algorithm are compared with the results obtained from PSO algorithm as tabulated in Table (2).

The obtained (I-V)-(P-V) characteristic curves based

on the proposed AOA for the three models are compared with experimental curves of PSO algorithm as shown in Figures (15-17).
It is observed that, the optimal extracted parameters of the study module have minimum SDM RMSE equals 0.062877, DDM RMSE with value 0.062415 and TDM RMSE 0.062696.

Table 2- Mono Crystalline 390 – 430 TS6S96 (TS-S410) SDM, DDM, TDM extracted parameters using AOA and PSO algorithm and root mean square error (RMSE).

	AOA			PSO Algorithm		
Variable	**SDM**	**DDM**	**TDM**	**SDM**	**DDM**	**TDM**
$I_{ph}(A)$	8.95376	8.94095	8.95763	8.9496771	8.9511954552	8.9497707063
$I_{o1}(\mu A)$	0.0348066	0.0314471	0.0229372	0.032742724	0.026703330	0.025130240
$R_s(\Omega)$	0.0003777	0.00013321	0.0000975	0.00039632	0.0003397681	0.00033969721
n_1	1.26126	1.31964	1.25066	1.257257425	1.25434	1.252561
$R_{sh}(\Omega)$	33.7929	32.6069	30.0255	45.09722	56.996232	59.5564071
$I_{o2}(\mu A)$	-	0.0250496	0.0126472	-	0.024068815	0.023369819
n_2	-	1.2705	1.31452	-	1.370884	1.3554363
$I_{o3}(\mu A)$	-	-	1.90878	-	-	0.025233525
n_3	-	-	1.92919	-	-	2.1920361
RMSE	0.062877	0.062415	0.062696	0.062918	0.06282	0.062806

Also, the (I-V)-(P-V) characteristic curves obtained by the identified model using the proposed AOA have the best agreement with the experimental results.

The results indicated that PSO has many drawbacks such as difficult to define initial design parameters, cannot work out dispersion problems, and converge prematurely and be trapped at a local minimum especially with complex problems and large networks [36].
AOA algorithm compared to PSO needs less running time in terms of seconds. Since AOA is a population-based algorithm, there is no need for optimization processes, i.e., Multiplication, Division, Subtraction, and Addition. Consequently, it is concluded that the computational performance of the proposed AOA algorithm is sufficiently better and efficient and the obtained results are more accurate than PSO.

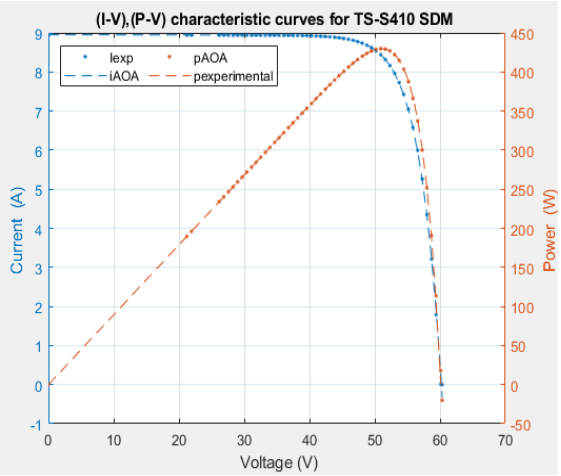

Figure 15- (I-V), (P-V) characteristic curves for Mono Crystalline 390 – 430 TS6S96 (TS-S410) SDM

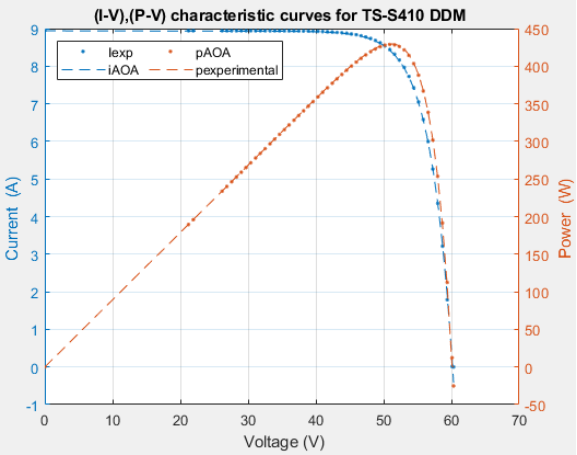

Figure 16- (I-V), (P-V) characteristic curves for Mono Crystalline 390 – 430 TS6S96 (TS-S410) DDM

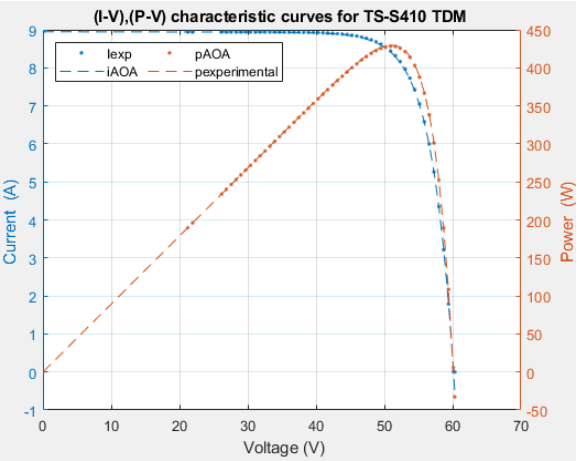

Figure 17- (I-V), (P-V) characteristic curves for Mono Crystalline 390 – 430 TS6S96 (TS-S410) TDM

5.2. Simulation Results of NREA 42 KW PV Power System.

The simulation output waveforms are appeared as illustrated in Figures (18-21) and the results of output energy are compared with the actual output energy of the system. Thus, the results explain that, the Simulink model of the 42 kW PV system is used to simulate of the real case study.

The simulation results are recorded for NREA 42 KW PV power system at the standard test conditions depend upon the selected solar panel specifications. All the blocks in the proposed design block diagram are simulated and the details of the circuit responses are collected.

The output DC current of the PV models (DC part) is shown in Fig. 18. However, the DC current is approximately 71.8 (A).

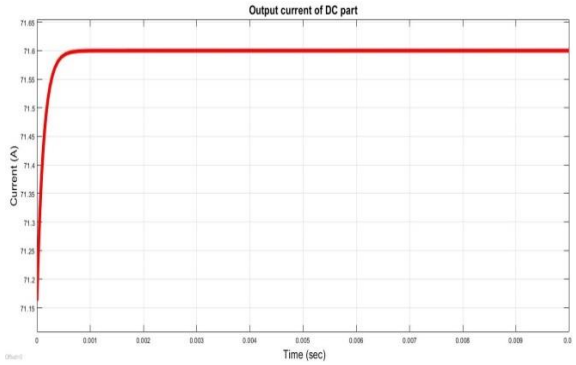

Figure 18- Output of the DC part

The output AC voltage of the inverter is shown in Figure (19), where the three-phase line to line voltages have sinusoidal wave shapes including some harmonics. The value of output voltage is close to the required one. Figure (20) shows the three-phase output voltage without harmonics by applying proper filter circuits. The three-phase output power injected into utility grid is shown as in Figure (21).

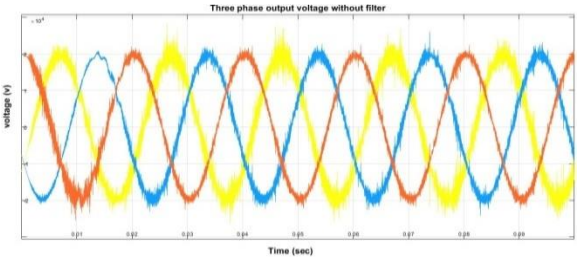

Figure 19- Three-phase output voltage without filter

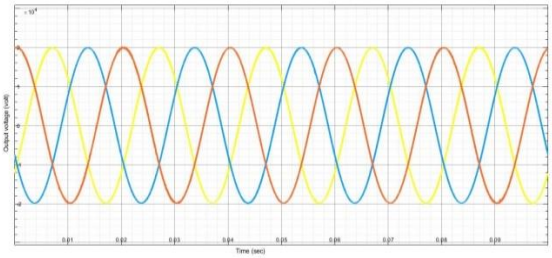

Figure 20- Three phase output voltage of NREA 42 KW PV power system without harmonics

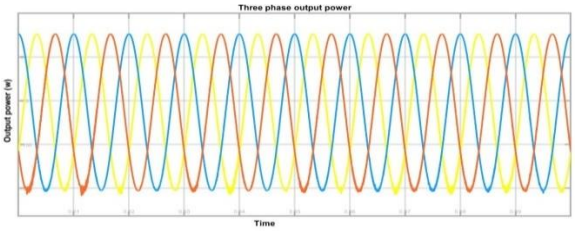

Figure 21- Three-phase output power injected into utility grid

5.3. Performance Analysis of the Results

Figure (22) shows a comparison between the simulation output energy and the actual monthly average energy injected into the grid in kWh. The maximum energy injected into the grid is in month of August-2020 with value of 224.366 KWh. Likewise, the minimum energy injected into the grid is in month of December-2020 with value of 117.645 kWh. The total energy injected into the grid is equal to 2173.07 kWh/year. The values of actual output energy and that obtained from the simulation results are illustrated in Table (3).

Table 3- Actual and simulated output Energy (Wh)

Date	Average output E (Wh)	Simulation results
20-Jan	138788.2903	149015.2903
20-Feb	164609.2857	175319.2857
20-Mar	164609.2857	169985.2857
20-Apr	206422.4	209861.4
20-May	199552.8	210691.8
20-Jun	233316.0333	229269.0333
20-Jul	222970.6452	234589.6452
20-Aug	224366.4516	235269.4516
20-Sep	193181.6	204897.6
20-Oct	165794.0968	175981.0968
20-Nov	141814.3	152036.3
20-Dec	117645.5806	128105.5806
Total output Energy	2173070.769	2275021.769
Average/year	181089.2308	189585.1474

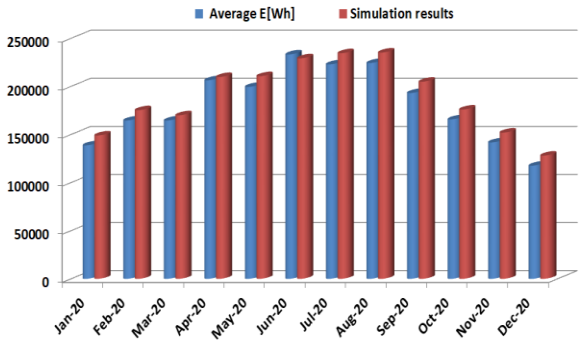

Figure 21- A comparison between the actual monthly energy injected into the grid in kWh and the simulation output energy

6. Conclusions

This paper proposes a mathematical model of different PV models (SDM, DDM and TDM) by a set of analytical equations. Arithmetic Optimization Algorithm (AOA) is proposed to extract optimal PV models parameters for minimizing error between the experimentally collected data and the theoretical data. From the results, it is observed that the obtained (P-V) and (I-V) characteristic curves using AOA have the best agreement with the experimental results compared to PSO algorithm.

According to the extracted optimal parameters of Mono Crystalline 390 – 430 TS6S96 (TS-S410) PV module, the detailed Simulink model has been designed for the study module to build a model of small-scale NREA 42 KW PV power system connected to the utility grid. The output energy is compared with the actual energy generated which is appeared on the inverter screen in the location site.

7. References

[1] Makarova, Arina. "Study, Design and Performance Analysis of a Grid-Connected Photovoltaic System: Case study: 5 MW Grid-Connected PV System in Namibia." (2017).

[2] H. Yehya. "Assessment the Influence of Grid Connected Photovoltaic System on Medium Voltage Network in Tubas." (2019).

[3] K., M. Mounir, and Mohamed Ibrahim Abdelall. "Ecological desert settlement Egypt western desert." Alexandria Engineering Journal 58.1 (2019): 291-301.

[4] Saifaddin Galal "Total solar energy capacity in Egypt" Mar 2, 2021. https://www.statista.com/statistics/1215515/egypt-total-solar-energy-capacity/,

[5] REN21 Members, Renewables 2021 - Global status report. 2021.

[6] I. Renewable and E. Agency, RENEWABLE.

[7] A. A. Zaky et al., "Optimal Performance Emulation of PSCs using the Elephant Herd Algorithm Associated with Experimental Validation," ECS J. Solid State Sci. Technol., vol. 8, no. 12, pp. Q249–Q255, 2019, doi: 10.1149/2.0271912jss.

[8] A. S. A. Bayoumi, R. A. El-Sehiemy, and A. Abaza, "Effective PV Parameter Estimation Algorithm Based on Marine Predators Optimizer Considering Normal and Low Radiation Operating Conditions," Arab. J. Sci. Eng., 2021, doi: 10.1007/s13369-021-06045-0.

[9] A. R. Ginidi, A. M. Shaheen, R. A. El-Sehiemy, and E. Elattar, "Supply demand optimization algorithm for parameter extraction of various solar cell models," Energy Reports, vol. 7, pp. 5772–5794, 2021, doi: https://doi.org/10.1016/j.egyr.2021.08.188.

[10] M. A. El-Dabah, R. A. El-Sehiemy, M. Becherif, and M. A. Ebrahim, "Parameter estimation of triple diode photovoltaic model using an artificial ecosystem-based optimizer," Int. Trans. Electr. Energy Syst., vol. n/a, no. n/a, p. e13043, doi: https://doi.org/10.1002/2050-7038.13043.

[11] Malki, A., Mohamed, A.A., Rashwan, Y.I., El-Sehiemy, R.A. and Elhosseini, M.A., 2021. Parameter Identification of Photovoltaic Cell Model Using Modified Elephant Herding Optimization-Based Algorithms. Applied Sciences, 11(24), p.11929.

[12] W. Long, S. Cai, J. Jiao, M. Xu, and T. Wu, "A new hybrid algorithm based on grey wolf optimizer and cuckoo search for parameter extraction of solar photovoltaic models," Energy Convers. Manag., vol. 203, no. June 2019, p. 112243, 2020, doi: 10.1016/j.enconman.2019.112243.

[13] L. Abualigah, A. Diabat, S. Mirjalili, M. Abd Elaziz, and A. H. Gandomi, "The Arithmetic Optimization Algorithm," Comput. Methods Appl. Mech. Eng., vol. 376, p. 113609, 2021, doi: 10.1016/j.cma.2020.113609.

[14] A. Benahmida, N. Maouhoub, and H. Sahsah, "Numerical approach for extraction of photovoltaic generator single-diode model parameters," Comput. Sci. Inf. Technol., vol. 2, no. 2, pp. 58–66, 2021, doi: 10.11591/csit.v2i2.p58-66.

[15] I. Bodnár, D. Koós, P. Iski, and Á. Skribanek, "Design and construction of a sun simulator for laboratory testing of solar cells," Acta Polytech. Hungarica, vol. 17, no. 3, pp. 165–184, 2020, doi: 10.12700/APH.17.3.2020.3.9.

[16] J. N. L. Naraharisetti, R. Devarapalli, and V. Bathina, "Parameter extraction of solar photovoltaic module by using a novel hybrid marine predators–success history based adaptive differential evolution algorithm," Energy Sources, Part A Recover. Util. Environ. Eff., vol. 00, no. 00, pp. 1–23, 2020, doi: 10.1080/15567036.2020.1806956.

[17] A. S. Bayoumi, R. A. El-Sehiemy, K. Mahmoud, M. Lehtonen, and M. M. F. Darwish, "Assessment of an improved three-diode against modified two-diode patterns of MCS solar cells associated with soft parameter estimation paradigms," Appl. Sci., vol. 11, no. 3, pp. 1–20, 2021, doi: 10.3390/app11031055.

[18] I. Bodnár, D. Matusz-Kalász, and D. Koós, "Experimental and numerical analysis of solar cell temperature transients," Pollack Period., vol. 16, no. 2, pp. 104–109, 2021, doi: 10.1556/606.2020.00260.

[19] I. Syazleen, A. Ridhor, Z. M. Isa, and N. M. Nayan, "Parameter Extraction of PV Cell Single Diode Model Using Animal Migration Optimization," 2020.

[20] X. Lin and Y. Wu, "Parameters identification of photovoltaic models using niche-based particle swarm optimization in parallel computing architecture," Energy, vol. 196, 2020, doi: 10.1016/j.energy.2020.117054.

[21] N. Pourmousa, S. M. Ebrahimi, M. Malekzadeh, and M. Alizadeh, "Parameter estimation of photovoltaic cells using improved Lozi map based chaotic optimization Algorithm," Sol. Energy, vol. 180, no. July 2018, pp. 180–191, 2019, doi: 10.1016/j.solener.2019.01.026.

[22] K. Yu, J. J. Liang, B. Y. Qu, X. Chen, and H. Wang, "Parameters identification of photovoltaic models using an improved JAYA optimization algorithm," Energy Convers. Manag., vol. 150, no. July, pp. 742–753, 2017, doi: 10.1016/j.enconman.2017.08.063.

[23] D. Yousri, M. Abd Elaziz, D. Oliva, L. Abualigah, M. A. A. Al-qaness, and A. A. Ewees, "Reliable applied objective for identifying simple and detailed photovoltaic models using modern metaheuristics: Comparative study," Energy Convers. Manag., vol. 223, no. June, 2020, doi: 10.1016/j.enconman.2020.113279.

[24] A. Elkholy and A. A. Abou El-Ela, "Optimal parameters estimation and modelling of photovoltaic modules using analytical method," Heliyon, vol. 5, no. 7, 2019, doi: 10.1016/j.heliyon.2019.e02137.

[25] K. Et-torabi et al., "Parameters estimation of the single and double diode photovoltaic models using a Gauss–Seidel algorithm and analytical method: A comparative study," Energy Convers. Manag., vol. 148, pp. 1041–1054, 2017, doi: 10.1016/j.enconman.2017.06.064.

[26] M. A. E. H. Mohamed, "The linear model of a PV moduel," Int. J. Power Electron. Drive Syst., vol. 8, no. 2, pp. 900–906, 2017, doi: 10.11591/ijpeds.v8i2.pp900-906.

[27] J. Ramos-Hernanz, I. Uriarte, J. M. Lopez-Guede, U. Fernandez-Gamiz, A. Mesanza, and E. Zulueta, "Temperature based maximum power point tracking for photovoltaic modules," Sci. Rep., vol. 10, no. 1, pp. 1–10, 2020, doi: 10.1038/s41598-020-69365-5.

[28] P. J. Gnetchejo, S. N. Essiane, P. Ele, R. Wamkeue, D. M. Wapet, and S. P. Ngoffe, "Enhanced Vibrating Particles System Algorithm for Parameters Estimation of Photovoltaic System," J. Power Energy Eng., vol. 07, no. 08, pp. 1–26, 2019, doi: 10.4236/jpee.2019.78001.

[29] B. Maniraj and A. Peer Fathima, "Parameter extraction of solar photovoltaic modules using various optimization techniques: A review," J. Phys. Conf. Ser., vol. 1716, no. 1, 2021, doi: 10.1088/1742-6596/1716/1/012001.

[30] M. Said et al., "Estimating parameters of photovoltaic models using accurate turbulent flow of water optimizer," Processes, vol. 9, no. 4, pp. 1–23, 2021, doi: 10.3390/pr9040627.

[31] A. M. Shaheen, A. R. Ginidi, R. A. El-Sehiemy, and S. S. M. Ghoneim, "A Forensic-Based Investigation Algorithm for Parameter Extraction of Solar Cell Models," IEEE Access, vol. 9, pp. 1–20, 2021, doi: 10.1109/ACCESS.2020.3046536.

[32] Z. Cen, "Modeling and Simulation for an 8 kW Three-Phase Grid-Connected Photo-Voltaic Power System," Open Phys., vol. 15, no. 1, pp. 603–612, 2017, doi: 10.1515/phys-2017-0070.

[33] H. Abobakr, A. Diab, Y. B. Hassan, and A. Khalaf, "Performance Analysis of a Small-Scale Grid-Connected Photovoltaic System:a Real Case Study in Egypt," J. Adv. Eng. Trends, vol. 40, no. 1, pp. 79–96, 2021, doi: 10.21608/jaet.2021.82233.

[34] S. S. Mohammed and D. Devaraj, "System with Boost Converter using," Int. Conf. Circuit, Power Comput. Technol. [ICCPCT], vol. 7, no. 14, pp. 814–821, 2014.

[35] G. Tambouratzis, "PSO Optimal Parameters and Fitness Functions in an NLP Task," 2019 IEEE Congr. Evol. Comput. CEC 2019 - Proc., pp. 611–618, 2019, doi: 10.1109/CEC.2019.8789914.

[36] Z. Abdmouleh, A. Gastli, L. Ben-Brahim, M. Haouari, and N. A. Al-Emadi, "Review of optimization techniques applied for the integration of distributed generation from renewable energy sources," Renewable Energy, vol. 113, pp. 266–280, 2017.

Appendix (A)